Single-Phase PrO_y-ZrO_2 Materials and Their Oxygen Storage Capacity: A Comparison with Single-Phase CeO_2-ZrO_2, PrO_y-CeO_2, and $PrO_y-CeO_2-ZrO_2$ Materials

C. K. Narula* and L. P. Haack

Chemistry Department, Ford Motor Company, MD3083/SRL, P.O. Box 2053, Dearborn, Michigan 48121

W. Chun, H.-W. Jen, and G. W. Graham*

Chemical Engineering Department, Ford Motor Company, MD3179/SRL, P.O. Box 2053, Dearborn, Michigan 48121

Received: November 10, 1998; In Final Form: February 18, 1999

High-surface-area PrO_y-ZrO_2 mixed oxide, crystallized in the cubic fluorite structure, is synthesized for the first time as a single-phase material over a wide range of composition by sol−gel processing. X-ray powder diffraction shows that the material remains single phase even after thermal treatment in air to 900 °C. The oxygen storage capacity of PrO_y-ZrO_2, where praseodymium undergoes $Pr^{3+} \leftrightarrow Pr^{4+}$ interconversion, is assessed by temperature-programmed reduction with H_2. The results show that there is little oxygen storage capacity unless the PrO_y concentration exceeds 25 mol %. A comparison of oxygen storage capacity from similarly prepared single-phase CeO_2-ZrO_2, PrO_y-CeO_2, and $PrO_y-CeO_2-ZrO_2$ materials is presented. Measurements of lattice parameter and reducibility suggest that there are preferred associations that lead to PrO_y-ZrO_2 and CeO_2-ZrO_2 rather than PrO_y-CeO_2 in the ternary mixed oxide. An evaluation of model Pd catalysts, using PrO_y-ZrO_2 and CeO_2-ZrO_2 as support materials, in functional tests approximating warmed-up, steady-state operation of an automotive catalyst, is also reported.

Introduction

Materials that can alternatively take up and release oxygen, i.e., provide oxygen storage, are useful in a number of diverse applications including catalytic oxidation,[1] separation of air,[2] and cryogenic refrigeration.[3] Among these materials, cerium oxide has received a great deal of attention,[4] especially in connection with automotive exhaust catalysis where its main function is to provide a buffer against imposed variations in air-to-fuel ratio.[5] In recent years, it has been found that cerium oxide containing zirconium oxide is much better than pure ceria, and several synthetic routes have been developed to prepare high-surface-area CeO_2-ZrO_2 mixed oxides.[6] The reasons for the greatly enhanced oxygen storage capacity and faster exchange kinetics of these materials, compared with pure cerium oxide, have yet to be fully understood.[6,7]

The development of such ceria-based mixed oxides has motivated new interest in mixed oxides containing the other rare-earth elements with variable oxidation state, Pr and Tb.[8−11] Like Ce, these form dioxides that crystallize in the cubic fluorite structure and tend to form solid solutions with other fluorite-type oxides. Their dioxides are of lower stability than ceria, however, allowing oxygen exchange to be effected at lower temperatures than in ceria. High-surface-area forms of praseodymia or praseodymia-based mixed oxides, analogous to ceria or ceria−zirconia, could possibly provide new oxygen storage materials with more easily accessible oxygen than in ceria.

In earlier exploratory work aimed at making and characterizing low-surface-area forms of mixed oxides of praseodymia with ceria and zirconia,[8,9] the preparation of PrO_y-ZrO_2 mixed oxides by coprecipitation methods led to materials crystallized in a mixture of cubic and tetragonal phases. In our present efforts to produce the corresponding high-surface-area materials, we found that sol−gel processing leads to single-phase PrO_y-ZrO_2 and $PrO_y-CeO_2-ZrO_2$ materials crystallized in the cubic fluorite structure. Here, we present results from their characterization. We also present results from similarly prepared CeO_2-ZrO_2 and PrO_y-CeO_2 materials. A comparison of oxygen storage capacity of these materials by temperature-programmed reduction is described. We also present our preliminary evaluation of one of the compositions of PrO_y-ZrO_2 as an oxygen storage material in a model Pd automotive catalyst.

Experimental Details

Oxides were synthesized by sol−gel processing methods and characterized using a variety of techniques. Thermogravimetric analysis and infrared spectroscopy were performed with Perkin-Elmer TGA7and System 2000 instruments, respectively. Specific surface areas were measured by the BET method using a Micromeritics ASAP 2400 instrument. Powder X-ray diffraction (XRD) patterns were obtained using a Scintag X1 diffractometer and Cu Kα radiation. X-ray photoelectron spectroscopy (XPS) with monochromatic Al Kα radiation was performed using a Kratos Axis 165 spectrometer with an attached sample treatment chamber.

General Method for the Preparation of Gels. The alkoxides of cerium, praseodymium, and zirconium were prepared by known methods.[12] A 100 mL flask was charged with appropriate alkoxides dissolved in THF (40 mL) for the preparation of PrO_y, CeO_2, $mPrO_y-nZrO_2$, $mCeO_2-nZrO_2$, $mPrO_y-nCeO_2$ ($\{m, n\} = \{1, 3\}$, $\{1, 1\}$, and $\{3, 1\}$), and $PrO_y-CeO_2-nZrO_2$ ($n = 1$, 2) gels. The reaction mixture was cooled to −78 °C and reacted

* Author for correspondence.

10.1021/jp984383n CCC: $18.00
Published on Web 04/20/1999

with water (1.0 mL) mixed with THF (20 mL). The gels formed immediately and were then dried by removing volatiles in vacuum. The resulting powders were pyrolyzed in air. As a specific example, the preparation of PrO_y-ZrO_2 was performed as follows: A 100 mL flask was charged with $Pr(O^iC_3H_7)_3$ (2.05 g) and $Zr(O^iC_3H_7)_4{\cdot}^iC_3H_7OH$ (2.5 g) dissolved in THF (40 mL). The reaction mixture was cooled to −78 °C and reacted with water (1.0 mL) mixed with THF (20 mL). The gel, thus obtained, was dried under vacuum and pyrolyzed in air at 400 °C to obtain 1.97 g of product.

Catalysts were made from a subset of the mixed-oxide materials, PrO_y-ZrO_2 and CeO_2-ZrO_2, after calcination at 600 °C, by impregnation with an organic precursor, $Pd(dba)_2$, to a nominal loading of 2 wt % Pd, followed by stepwise calcination up to 600 °C for 1 h.

Temperature-Programmed Reduction. Reducibility of the mixed-oxide materials was probed by temperature-programmed reduction (TPR) measurements using hydrogen (in argon) in an Altamira system employing a thermal conductivity detector. The standard pretreatment involved heating the powder sample (typically 100 mg) at 500 °C for 1 h in a flowing mixture of 10% oxygen in helium to ensure full oxidation. The sample was then cooled to room temperature in the flowing oxygen/helium gas. After switching to a feed gas of 9.4% hydrogen in argon, the TPR trace was acquired by ramping the sample temperature up to 900 °C at a rate of 10 deg/min. Hydrogen consumption (expressed in μmol of H_2/g of sample) was quantified by integrating the areas under the peaks, utilizing sensitivity factors measured after each run (from injection of known quantities of the hydrogen/argon gas).

Dynamic Oxygen Storage Capacity on Pulsed Microreactor. Dynamic oxygen storage capacity measurements of a more functional nature were performed on two catalysts using a lab-built mass-spectrometer-based pulsed microreactor.[7] Samples of the catalysts were prepared by pressing thin disks from powders and breaking the disks into small pieces that were loaded into a quartz U-tube reactor. Prior to an oxygen storage measurement, the sample was first heated at the desired test temperature for at least 20 min in 0.5% oxygen in helium. The sample was then exposed to alternating pulses of 0.5% oxygen in helium and 1% carbon monoxide in helium, with pulses of pure helium interspersed to purge any remnant gas-phase species. The dynamic oxygen storage capacity (OSC) was quantified in terms of μmol of O atoms/g of catalyst by comparing integrated amounts of CO in pulses entering and exiting the reactor. Close agreement was obtained between OSC values calculated from consumption of CO and those calculated from either production of CO_2 or consumption of O_2 (during reoxidation of the catalyst).

Results and Discussion

The equilibrium phase diagram of praseodymium oxide−zirconium oxide shows that at a concentration of praseodymium oxide below 40%, monoclinic and cubic phases are observed.[13] This mixture of phases transforms to tetragonal and cubic phases in the 1000−1500 °C range and to a fluorite-structured phase in the 1500−2200 °C range depending on the concentration of PrO_y. For concentrations of PrO_y in the 42−56% range, a pyrochlore phase is observed. Above 56%, the material is a mixture of pyrochlore and tetragonal phases. Among these phases, PrO_y-ZrO_2 crystallized in the fluorite structure is expected to be useful for oxygen storage since it should allow $PrO_2-PrO_{1.5}$ interchange.

In an earlier study, the preparation of PrO_y-ZrO_2 materials by coprecipitation from aqueous solutions of the metal nitrates was reported.[9] The resulting materials crystallized in a mixture of fluorite and tetragonal phases. The fraction of material with cubic fluorite structure depended on the concentration of ZrO_2 in the system. Here, in our effort to prepare high-surface-area materials by an alternate synthetic route, we found that the green material produced upon pyrolysis of the gels derived from mixtures of $Pr(O^iC_3H_7)_3$ and $Zr(O^iC_3H_7)_4{\cdot}^iC_3H_7OH$ in 1:3, 1:1, and 3:1 molar ratios were all single phase, having the cubic fluorite structure. The high-resolution electron micrographs of powder shows that they comprise 5 nm particles. The Pr:Zr peak intensities in energy dispersive spectra do not vary from particle to particle.[14] Further heating at 600 °C in air caused these powders to turn black, but they retained their structure and phase purity.

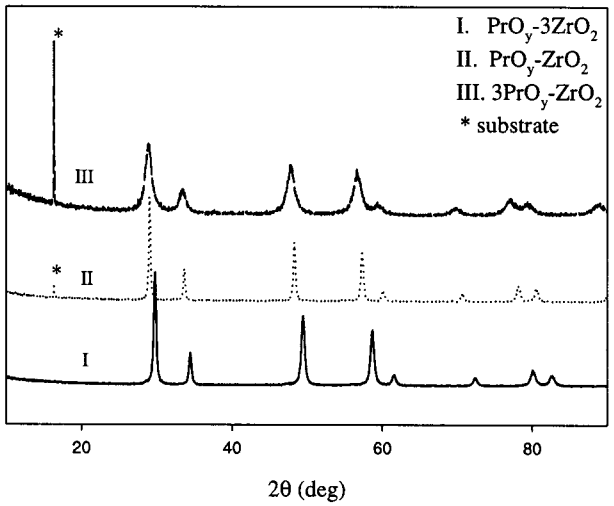

Figure 1. XRD patterns of PrO_y-ZrO_2 materials calcined at 900 °C.

The gels prepared from various mixtures of $Pr(O^iC_3H_7)_3$, $Ce(O^iC_3H_7)_4$, and $Zr(O^iC_3H_7)_4{\cdot}^iC_3H_7OH$, aimed at making PrO_y, CeO_2, $mCeO_2-nZrO_2$, and $mPrO_y-nCeO_2$ ($\{m, n\} = \{1, 3\}$, $\{1, 1\}$, and $\{3, 1\}$) materials by the same sol−gel method, also yielded single-phase cubic fluorite-structured powders upon pyrolysis, as did the gels derived from mixtures of $Pr(O^iC_3H_7)_3$, $Ce(O^iC_3H_7)_4$, and $Zr(O^iC_3H_7)_4{\cdot}^iC_3H_7OH$ in 1:1:1 and 1:1:2 molar ratios.

Thermogravimetric analysis of all the gels in air showed that weight loss was complete at 400 °C. The specific surface areas of the residues at this stage were in the range 80−120 m^2/g (BET). After calcination at 600 °C, the surface areas were typically lower by a factor of 2. A final calcination at 900 °C was performed before most of the characterization; catalysts, however, were not calcined above 600 °C in order to maintain a reasonably high surface area.

Powder X-ray diffraction patterns of the PrO_y-ZrO_2 materials with 1:3, 1:1, and 3:1 molar ratios, all displaying only diffraction peaks due to the cubic fluorite-type structure, are shown in Figure 1. This result is certainly distinct from that obtained earlier by Sinev and co-workers where a mixture of phases was observed throughout the midrange of compositions.[9] The patterns from the CeO_2-ZrO_2 materials shown in Figure 2, which evolve from cubic to tetragonal in character with increasing ZrO_2 concentration, are as expected.[15] Simiarly, the patterns from the PrO_y-CeO_2 materials, as well as the pure oxides, shown in Figure 3, also conform to expectation.[16]

The lattice constants derived from these patterns are plotted in Figures 4−6 along with literature values for various pure oxides. The lines, drawn by assuming a linear variation with composition, are consistent with estimates made according to

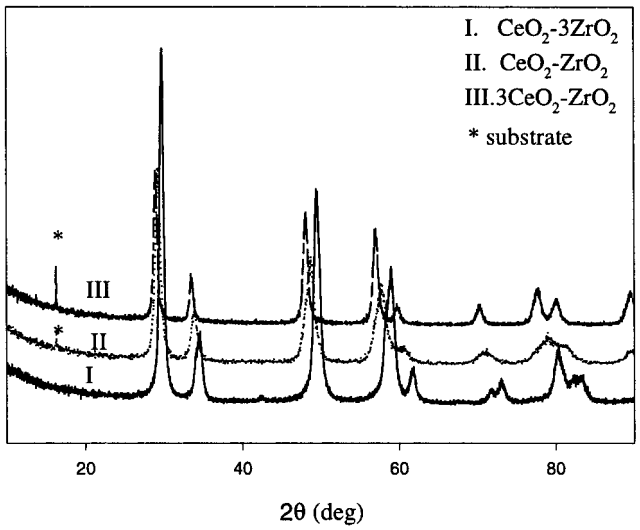

Figure 2. XRD patterns of CeO_2-ZrO_2 materials calcined at 900 °C.

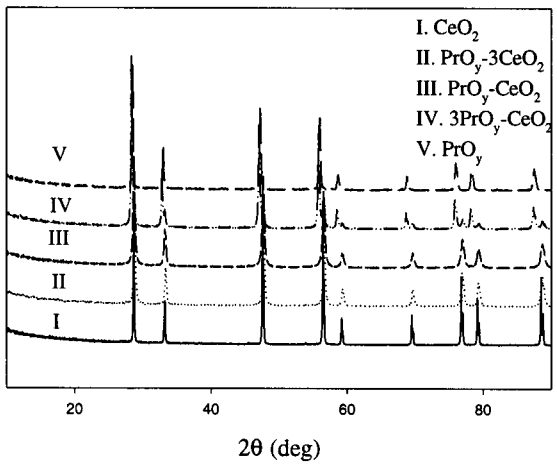

Figure 3. XRD patterns of PrO_y-CeO_2 materials calcined at 900 °C.

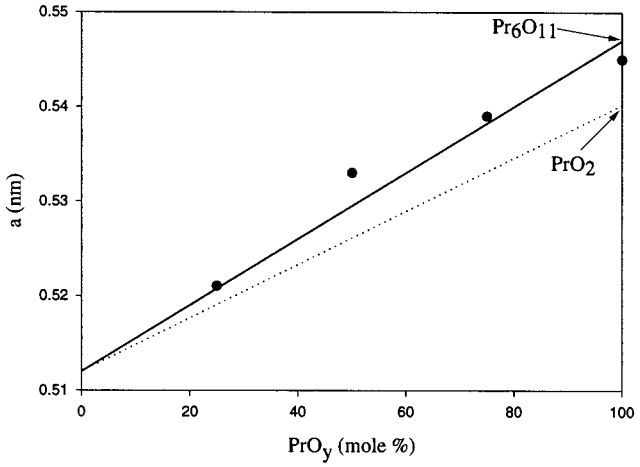

Figure 4. Lattice parameters of PrO_y-ZrO_2 materials.

Kim.[17] The correspondence in Figure 4 suggests that the praseodymium in the PrO_y-ZrO_2 materials is a mixture of Pr^{4+} and Pr^{3+}, close to that in Pr_6O_{11}. The break at a Pr-to-Ce ratio of 3 in Figure 6 marks the transition from praseodymium, which is fully Pr^{4+} to that which is a mixture of Pr^{4+} and Pr^{3+} (again, close to that in Pr_6O_{11}) in the PrO_y-CeO_2 materials, as known previously.[16] Comparison of the lattice constants derived from the XRD patterns produced by the PrO_y-CeO_2-ZrO_2 (0.536 nm) and $PrO_y-CeO_2-2ZrO_2$ (0.531 nm) powders, shown in Figure

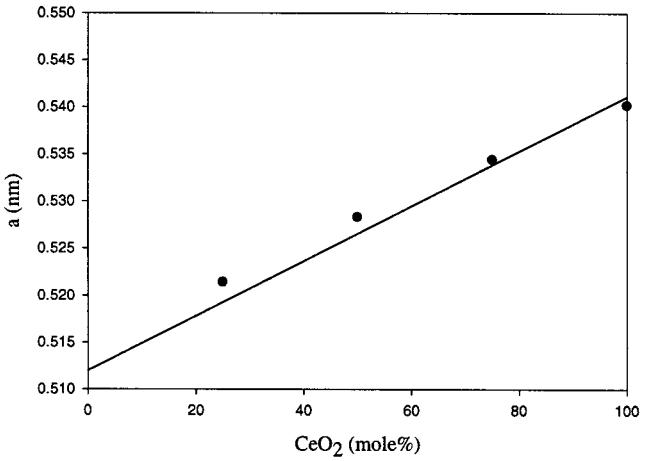

Figure 5. Lattice parameters of CeO_2-ZrO_2 materials.

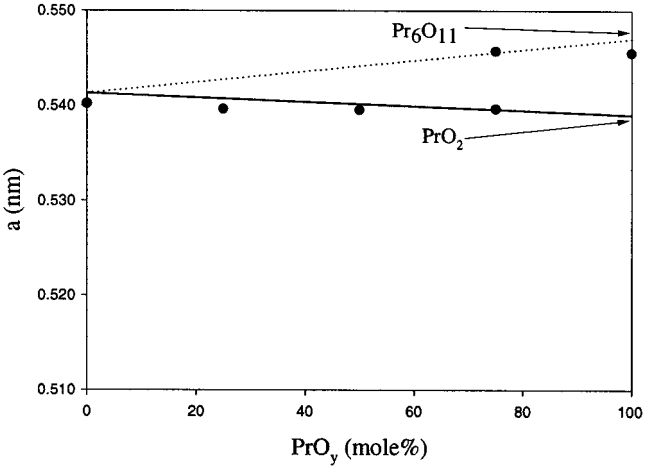

Figure 6. Lattice parameters of PrO_y-CeO_2 materials.

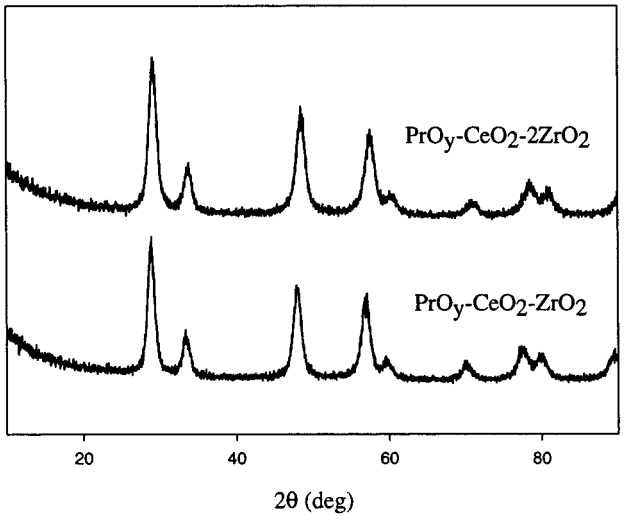

Figure 7. XRD patterns of $PrO_y-CeO_2-ZrO_2$ and $PrO_y-CeO_2-2ZrO_2$.

7, with the lines in Figure 4 suggests that the praseodymium in these mixed oxides is also a mixture of Pr^{4+} and Pr^{3+}, although the crystallinity in these materials is much lower than in any of the other praseodymium-containing materials. (The particle size in both materials is about 15 nm as calculated by Scherrer's formula, even after calcination at 900 °C, compared with about 40 nm in the PrO_y-ZrO_2 material, for example.)

The XPS results, shown in Figure 8, suggest that there is a difference in the relative amount of Pr^{4+} (i.e., $Pr^{4+}/(Pr^{3+}$ +

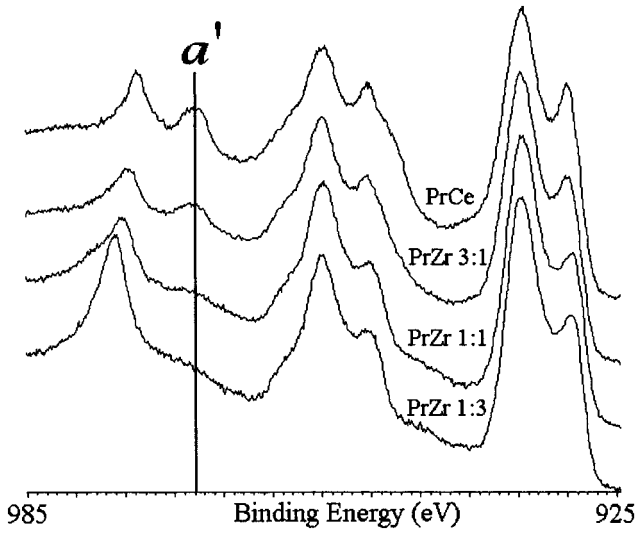

Figure 8. Pr 3d core level XPS of PrO_y-ZrO_2 materials calcined at 900 °C.

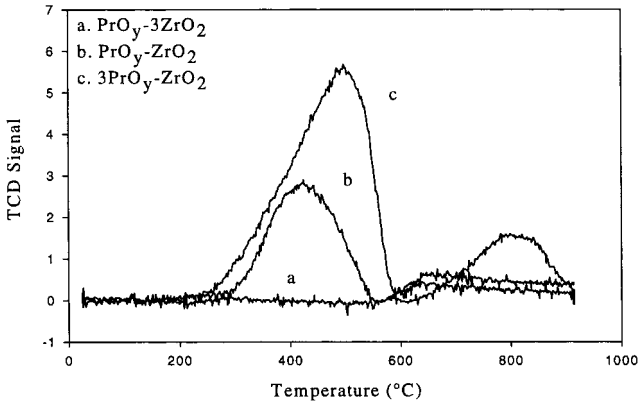

Figure 9. TPR of PrO_y-ZrO_2 materials calcined at 900 °C.

Pr^{4+})) among the various PrO_y-ZrO_2 materials, however, at least on the surface of the materials. These Pr 3d spectra were acquired after an additional oxidative treatment (450 °C in O_2) in the XPS reactor chamber. The feature at 968.0 eV, designated a′, is unique to Pr^{4+}. The Pr 3d spectrum of the 1:3 material is thus characteristic of pure Pr^{3+}, while that of the 1:1 material reveals a small amount of Pr^{4+}. The spectrum of the 3:1 material reveals at least twice as much Pr^{4+} as in the 1:1 material. That of $Pr_{0.55}Ce_{0.45}O_2$ provides a reference in which the amount of Pr^{4+} is maximal.[8]

The TPR traces of the PrO_y-ZrO_2 materials, shown in Figure 9, display only a weak broad peak above 550 °C (185 μmole H_2/g) for 1:3, two resolved peaks, one centered at 425 °C (428 μmol of H_2/g) and theother above 550 °C (169 μmole H_2/g) for 1:1, and two resolved peaks, one centered at 500 °C (825 μmoles H_2/g) and the other at 800 °C (153 μmole H_2/g) for 3:1. The relative reducibility of the various PrO_y-ZrO_2 materials thus appears to correlate roughly with the relative amount of Pr^{4+} present according to XPS. By comparison, TPR traces from the CeO_2-ZrO_2 materials, shown in Figure 10, display essentially one feature centered near 670 °C with an integrated area that is not very dependent on *m*:*n* (827−1072 μmol of H_2/g). Although the low-temperature reducibility is not simply proportional to the amount of PrO_y, these results demonstrate that the PrO_y-ZrO_2 materials can release oxygen at a lower temperature than the CeO_2-ZrO_2 materials.

The TPR traces of the sol−gel prepared CeO_2, PrO_y-3CeO_2, PrO_y-CeO_2, $3PrO_y-CeO_2$, and PrO_y samples, shown in Figure

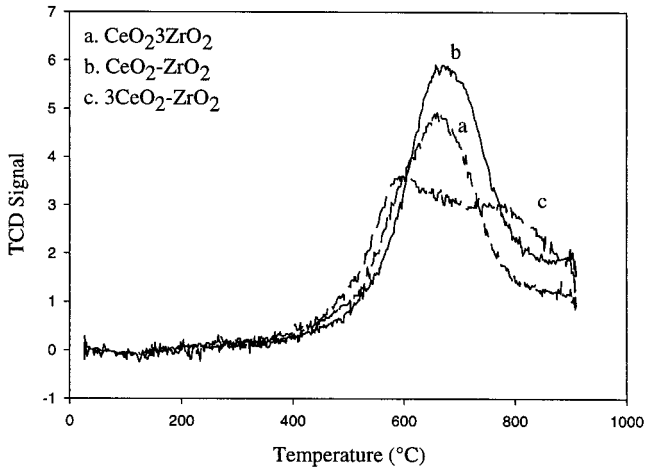

Figure 10. TPR of CeO_2-ZrO_2 materials calcined at 900 °C.

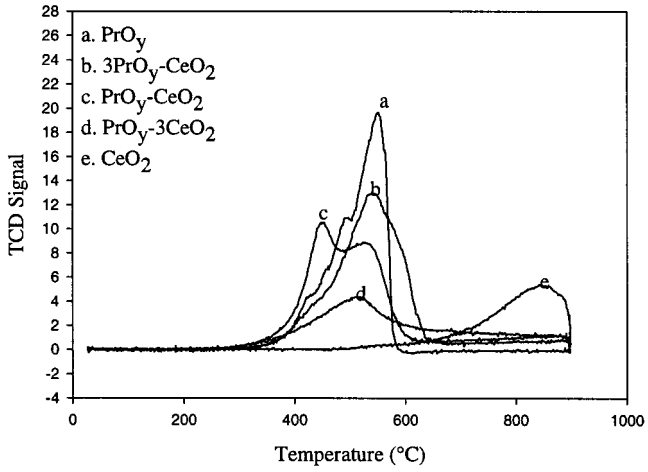

Figure 11. TPR of PrO_y-CeO_2 materials calcined at 900 °C.

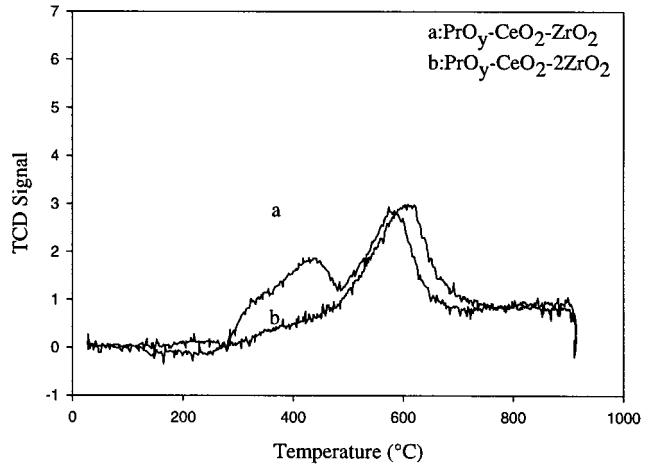

Figure 12. TPR of $PrO_y-CeO_2-nZrO_2$ materials calcined at 900 °C.

11, are not significantly different from those previously reported for these materials prepared by coprecipitation.[8] Interestingly, the reduction temperature of the PrO_y-CeO_2 materials is roughly intermediate to that of the PrO_y-ZrO_2 and the CeO_2-ZrO_2 materials. The TPR traces of the $PrO_y-CeO_2-ZrO_2$ materials, shown in Figure 12, contain a structure that resembles a superposition of that found in the TPR traces of PrO_y-ZrO_2 and CeO_2-ZrO_2, suggesting that these associations that are more favorable in the ternary mixed oxide than that of PrO_y-CeO_2. This is consistent with the XRD results, where the praseodymium appeared to be less than fully Pr^{4+}.

TABLE 1: Integrated TPR Results (where $RE_xZr_{1-x}O_z \rightarrow RE_xZr_{1-x}O_{z-\delta}$ upon TPR)

sample	H_2-uptake (μmol/g)	δ	δ/x
PrO_y-3ZrO_2	185	0.025	0.10
PrO_y-ZrO_2	597	0.088	0.18
$3PrO_y-ZrO_2$	978	0.16	0.21
PrO_y	1387	0.24	0.24
CeO_2-3ZrO_2	827	0.11	0.45
CeO_2-ZrO_2	1072	0.16	0.32
$3CeO_2-ZrO_2$	1031	0.16	0.22
CeO_2	696	0.12	0.12
PrO_y-3CeO_2	855	0.15	0.15
PrO_y-CeO_2	1427	0.25	0.25
$3PrO_y-CeO_2$	1221		
PrO_y-CeO_2-ZrO2	633	0.10	0.15
$PrO_y-CeO_2-2ZrO_2$	511	0.075	0.15

The H_2-uptake results from all the TPR measurements are summarized in Table 1. Assuming that $y \cong 1.83$ for all the single-phase materials (i.e., all but $3PrO_y-CeO_2$) except PrO_y-3CeO_2 and PrO_y-CeO_2, for which $y \cong 2$, as suggested by the XRD results, the H_2 uptakes may also be expressed in terms of δ or δ/x, defined by

$$RE_xZr_{1-x}O_z \rightarrow RE_xZr_{1-x}O_{z-\delta}$$

which relates to the TPR reaction. (In fact, the derived values of δ are not very sensitive to the precise values assumed for y.) These quantities, also listed in Table 1, are more useful for assessing and comparing the effect of Zr^{4+} incorporation in the two binary mixed oxides. In the case of the PrO_y-ZrO_2 materials, the addition of Zr^{4+}clearly decreases the reducibility, expressed as δ/x, while just the opposite is true in the case of the CeO_2-ZrO_2 materials. This well-known behavior in the latter case,[10] understood to imply that the addition of Zr^{4+} promotes the $Ce^{4+} \rightarrow Ce^{3+}$ reaction upon TPR, may also be viewed as a Zr^{4+}-induced destabilization of Ce^{4+} in the initial state (prior to TPR) of the mixed oxide relative to that in pure CeO_2. Evidence for slight initial reduction in CeO_2-ZrO_2 mixed oxides has, indeed, been obtained from XPS measurements.[18] Similarly, Pr^{4+} in the PrO_y-ZrO_2 materials also appears to have been destabilized by the addition of Zr^{4+}, according to the XPS results, but possibly to a much greater degree, allowing the relative amount of Pr^{4+} in the initial state to fall below that in Pr_6O_{11}. (A progressive decrease in the initial-state value of y with increasing Zr^{4+} fraction may not be evident from the XRD results since their sensitivity to the Pr oxidation state decreases with increasing Zr^{4+} fraction.) Thus, Zr^{4+} addition may be viewed as destabilizing RE^{4+} in both cases, but to different degrees: The slight destabilizationof Ce^{4+} serves to promote the $Ce^{4+} \rightarrow Ce^{3+}$ TPR reaction, but the much larger destabilization of Pr^{4+} results in a smaller relative amount of Pr^{4+} in the initial state before the TPR reaction. Consequently, Zr^{4+} addition produces opposite effects on the overall reducibilities of the two binary mixed oxides.

Functional tests approximating warmed-up, steady-state operation of an automotive catalyst, performed in the microreactor using alternating O_2 and CO pulses, were performed on Pd catalysts made with the 1:1 PrO_y-ZrO_2 and CeO_2-ZrO_2 materials. Results of measurements, using long (50 s) pulses, at 350 and 500 °C are listed in Table 2. Since the overall reducibility of the PrO_y-ZrO_2 material is about a factor of 2 smaller than that of the CeO_2-ZrO_2 material (according to Table 1), the observed ordering of their OSC's is to be expected. The actual ratio of the OSC's, 2.75 at 350 °C and 3.65 at 500 °C, is too large to be explained merely in terms of the difference in reducibility of the two materials, however, especially since a part of the total OSC in each case can be ascribed to the PdO/Pd redox reaction. The fact that the OSC of PrO_y-ZrO_2 is smaller at 500 °C than 350 °C probably reflects the falling thermodynamic stability of praseodymia, suggesting that the ability of this material to hold oxygen, even under slightly oxidizing conditions, may be limiting its dynamic OSC in this temperature range.[9]

TABLE 2: Dynamic Oxygen Storage Capacities for Pd Supported on 1:1 PrO_y-ZrO_2 and CeO_2-ZrO_2 Materials (50 s Pulses)

	oxygen storage capacity (μmol of O/g)	
sample	350 °C	500 °C
PrO_y-ZrO_2	333	283
CeO_2-ZrO_2	915	1034

TABLE 3: Dynamic Oxygen Storage Capacities for Pd Supported on 1:1 PrO_y-ZrO_2 and CeO_2-ZrO_2 Materials (10 s Pulses)

	oxygen storage capacity (μmol of O/g)	
temp (°C)	PrO_y-ZrO_2 1st/5th pulse	CeO_2-ZrO_2 1st/5th pulse
100	25/18	108/45
250	126/55	265/254
300	259/136	414/402
350	305/203	462/453

Results of additional measurements, using short (10 s) pulses at lower temperatures, are lister in Table 3. The first value is derived from the first CO pulse after peroxidation and the second derived from the fifth pair of $CO-O_2$ pulses in the sequence. The fifth pair of pulses represents a steady-state balance between the kinetics of reduction and reoxidation: At 100 °C, both of the materials provide greater OSC in the first than the fifth pulse, probably because of limitations due to reoxidation kinetics. At 250 °C and above, this pulse dependence largely disappears in the case of CeO_2-ZrO_2, indicating that reoxidation is fast on the time scale of the measurement. The increasing values of OSC with increasing temperature, on the other hand, reflect a continuing increase in the kinetics of oxygen release. (The values at 350 °C in the case of CeO_2-ZrO_2 are actually limited by the 10 s pulse length.) The ratio of OSC between CeO_2-ZrO_2 and PrO_y-ZrO_2, taken from the first pulse in the temperature range 250−300 °C, is now about 2, more in line with expectations based on relative overall reducibilities. The difference between OSC derived from the first and fifth CO pulses in the case of PrO_y-ZrO_2 in this temperature range is, again, probably a reflection of kinetic limitations that persist in this material because of the lower thermodynamic driving force toward reoxidation.[19]

Further evaluation of these praseodymium-based mateials in automotive catalyst applications, which can make use of their low-temperature release of oxygen, is in progress. The results will be presented in a future report.

Conclusions

We have shown that single-phase PrO_y-ZrO_2 and $PrO_y-CeO_2-ZrO_2$ materials crystallized in a cubic fluorite structure can be prepared by a sol−gel process employing a mixture of praseodymium, cerium, and zirconium alkoxides. Measurements of lattice constant and reducibility suggest, however, that there tend to be preferred associations that lead to PrO_y-ZrO_2 and CeO_2-ZrO_2 rather than PrO_y-CeO_2 in the ternary mixed oxide. The oxygen storage capacity of PrO_y-ZrO_2 materials, as gauged by H_2 reducibility, increases nonlinearly with PrO_y concentra-

tion, starting above 25 mol %. Reduction temperatures follow the sequence $PrO_y-ZrO_2 < PrO_y-CeO_2 < CeO_2-ZrO_2$. Differences in the dynamic OSC between Pd catalysts made with PrO_y-ZrO_2 and CeO_2-ZrO_2, observed in a functional test approximating warmed-up, steady-state operation of an automotive exhaust catalyst, appear to reflect differences in reoxidation kinetics and thermodynamic stability.

Acknowledgment. The authors gratefully acknowledge R. W. McCabe, who was involved in the early stages of this work, for his helpful comments on the manuscript, M. Yu. Sinev for his suggestions about interpreting the TPR data, and one of the reviewers for pointing out the usefulness of presenting the H_2-uptake results in terms of δ and δ/x.

References and Notes

(1) Sinev, M. Yu.; Bychkov, V. Yu.; Korchak, V. N.; Krylov, O. V. *Catal. Today* **1990**, *6*, 543.

(2) Mulhaupt, J. T.; Waldwick, N. J. U.S. Patent 3 980 763, 1976.

(3) Jones, J. A.; Blue, G. D. *J. Spacecraft* **1988**, *25*, 202.

(4) Trovarelli, A. *Catal. Rev.-Sci. Eng.* **1996**, *38*, 439.

(5) Narula, C. K.; Allison, J. E.; Bauer, D. R.; Gandhi, H. S. *Chem. Mater.* **1996**, *8*, 984.

(6) E.g.: Trovarelli, A.; Zamar, F.; Llorca, J.; de Leitenburg, C.; Dolcetti, G.; Kiss, J. T. *J. Catal.* **1997**, *169*, 490.

(7) Jen, H.-W.; Graham, G. W.; Chun, W.; McCabe, R. W.; Cuif, J.-P.; Deutsch, S. E.; Touret, O. *Catal. Today* **1999**, *50*, 309.

(8) Logan, A. D.; Shelef, M. *J. Mater. Res.* **1994**, *9*, 468.

(9) Sinev, M. Yu.; Graham, G. W.; Haack, L. P.; Shelef, M. *J. Mater. Res.* **1996**, *11*, 1960.

(10) Zamar, F.; Trovarelli, A.; de Leitenburg, C.; Dolcetti, G. *Stud. Surf. Sci. Catal.* **1996**, *101*, (11th International Congress on Catalysis, 40th Anniversary), 1283−1292.

(11) Bernal, S.; Blanco, G.; Cauqui, M. A.; Corchado, P.; Pintado, J. M.; Rodriguez-Izquierdo, J. M.; Vidal, H. *Stud. Surf. Sci. Catal.* **1998**, *116* (Catalysis and Automotive Pollution Control IV), 611−618.

(12) Bradley, D. C.; Mehrotra, R. C.; Gaur, D. P. *Metal Alkoxides*; Academic Press: London, 1978.

(13) Krasil'nikov, M. D.; Vinokurov, I. V.; Nikitina, S. D. *Fiz. Khim. Electrokhim. Rasplavl. Tverd. Electrolitov, Tezisy Dokl. Vses. Konf. Fiz. Khim. Ionnykh Rasplanov Tverd. Electrolitov* **1979**, *3*, 123.

(14) Narula, C. K.; Allard, L.; Graham, G. W. Unpublished results.

(15) Fornasiero, P.; Balducci, G.; DiMonte, R.; Kaspar, J.; Sergo, V.; Gubitosa, G.; Ferroer, A.; Graziani, M. *J. Catal.* **1996**, *164*, 173.

(16) Sovestnov, A. E.; Shaburov, V. A.; Melekh, B. T.; Smirnov, I. A.; Smirnov, Yu. P.; Tyunis, A. V.; Egorov, A. I. *Phys. Solid State* **1994**, *36*, 620.

(17) Kim, D.-J. *J. Am. Ceram. Soc.* **1989**, *72*, 1415.

(18) Galtayries, A.; Sporken, R.; Riga, J.; Blanchard, G.; Caudano, R. *J. Electron Spectrosc. Relat. Phenom.* **1998**, *88*−*91*, 951.

(19) Putna, E. S.; Vohs, J. M.; Gorte, R. J. Graham, G. W. *Catal. Lett.* **1998**, *54*, 17.